ACES Asian Chemical Editorial Society

doi.org/10.1002/asia.202401060

CHEMISTRY AN ASIAN JOURNAL Research Article

www.chemasianj.org

Development of Cyclometalated Iridium(III) Complexes of 2-Phenylbenzimidazole and Bipyridine Ligands for Selective Elimination of Gram-Positive Bacteria

Aryan Gautam,[a] Ajay Gupta,[a] Puja Prasad,[b] and Pijus K. Sasmal*[a]

Herein, we have reported a series of cationic aggregation-induced emission (AIE) active iridium(III) complexes (**Ir1-Ir5**) of the type $[Ir(CN)_2(NN)]Cl$, wherein CN is a cyclometalating 2-phenylbenzimidazole ligand with varying alkyl chain lengths and NN is a 2,2′-bipyridine ligand attached to bis-polyethylene glycol chains, for the treatment of bacterial infections. The AIE phenomenon of the complexes leveraged for detecting bacteria by fluorescence microscopy imaging that displayed a strong red emission in Gram-positive bacteria. The antibacterial activity of the complexes assessed against Gram-positive methicillin-sensitive *S. aureus*, methicillin-resistant *S. aureus*, *E. faecium* and *E. faecalis* and Gram-negative *E. coli* and *P. aeruginosa* bacteria of clinical interest. The complexes **Ir2-Ir4** exerted potent antibacterial activity towards Gram-positive strains with low minimum inhibitory concentrations (MICs) values in the range of 1–9 μM, which is comparable to clinically approved antibiotic vancomycin. In contrast, these complexes were found to be inactive towards Gram-negative bacterial strains (MICs >100 μM). The mechanism of antibacterial activity of the complexes implies that ROS generation, membrane depolarization and rupture are responsible for bacterial cell death. Further, the complexes **Ir1-Ir3** were found to be low-toxic against human red blood cells and human embryonic kidney (HEK293) cells, indicating their potential for use as antibacterial agents.

Introduction

Bacterial infections have emerged as a significant global concern, impacting millions of people worldwide.[1–3] The development of antibiotics have revolutionized medicine, with the discovery of penicillin marking the beginning of a new era in medicine. However, the rapid development of bacterial resistance to most of the existing antibiotics poses a serious public health threat. In 2019, over 1.3 million deaths are estimated from antimicrobial resistance (AMR), which is bound to increase if no new antibiotics are discovered.[1–5] Medicinal chemists mainly focus on the modification of existing antibiotics, which may only have a limited impact in the short term since pathogens adapt and become resistant to these modified antibiotics. Recently, Frei *et al.* highlighted that approx. 75% of the antimicrobial agents currently in clinical development are simply derivatives of already approved antibiotics.[6] This underscores the importance to design entirely novel classes of compounds with unique modes of action to combat AMR.

The World Health Organization (WHO) has listed ESKAPE bacteria as critical and high priority pathogens since they are insensitive to common antibacterial treatments.[2,7] Among these, *Staphylococcus aureus* (*S. aureus*) is one of the prevalent Gram-positive human pathogens that induce a variety of infectious diseases. Moreover, the emergence and increase in resistance of Gram-positive methicillin-resistant *S. aureus* (MRSA) against many antibiotics leads to a high mortality rate.[8,9] Additionally, MRSA has become a major nosocomial pathogen in many hospitals worldwide which has become a growing public health concern.[9,10] Therefore, there is a persuasive demand for the development of novel and potent antibacterial agents for treating *S. aureus* infections. Over the past few years, significant effort has been made in designing metal complexes for eradicating bacterial infections and AMR.[11–20] The metal complexes that possess antibacterial capabilities have been termed "metalloantibiotics". Metalloantibiotics are underexplored compounds that have gained considerable traction as potential antimicrobial agents in recent years.[21] Metal complexes with their three-dimensional shapes provide access to interact with different target sites of bacteria and offer a variety of modes of actions such as redox activation, ligand exchange or release, reactive oxygen species (ROS) generation, catalytic generation of toxic species *etc.*, which makes them superiors over organic scaffolds in combating AMR.[1,6]

Recently, metal-based aggregation-induced emission luminogens (AIEgens) with metal ions, such as Ir(III),[1,22–28] Ru(II),[29] Pt(II),[30–32] Zn(II),[33,34] have shown great promise as antimicrobial theranostic agents. Among these, cationic cyclometalated Ir(III) AIEgen complexes have earned significant attention due to their various advantages like kinetic inertness, positive charges, rich photophysical and photochemical properties, and generation of high levels of ROS, which make them promising candidates for detection, imaging and killing of bacterial infections.[1,22–26] Recently, our group has reported AIE-active

[a] *A. Gautam, A. Gupta, P. K. Sasmal*
School of Physical Sciences, Jawaharlal Nehru University, New Delhi 110067, India
E-mail: pijus@mail.jnu.ac.in

[b] *P. Prasad*
Amity Institute of Click Chemistry Research and Studies, Amity University, Noida, Uttar Pradesh 201303, India

Supporting information for this article is available on the WWW under https://doi.org/10.1002/asia.202401060

cationic cyclometalated Ir(III) complexes of 2-phenylquinoline and bipyridine ligands that exhibits simultaneous detection and eradication of drug-resistant bacteria.[23] Chen, Wong and co-workers have investigated AIE-active Ir(III) complexes with cyclometalating phenylpyridine and phenylquinoline ligands for fluorescence imaging and photodynamic inactivation of both Gram-positive and Gram-negative bacteria through ROS generation.[24] On the other hand, Wang *et al.* developed AIE-active cyclometalated Ir(III) photosensitizers for selective detection, imaging, and eradication of Gram-positive bacteria.[25] To date, there are reports on Ir(III) complexes with cyclometalating phenylquinoline, phenylpyridine, phenylbenzothiazole, and (2,4-difluorophenyl)pyridine ligands as bacterial imaging and therapeutic agents.[22–26] In contrast, there is only a single report of cyclometalated Ir(III) complexes with biologically important phenylbenzimidazole ligands as antibacterial agents.[35] For this, Ruiz and co-workers have disclosed Ir(III) complexes with cyclometalating 2-phenylbenzimidazole, and NN donor phenanthroline ligands demonstrating efficient antibacterial activity selectively against Gram-positive bacteria. The mechanism of antibacterial activity of these complexes is mainly due to ROS generation while without affecting the cell wall and membrane or damaging DNA of the bacteria.[35] However, there is no report on iridium AIEgens coordinated with 2-phenylbenzimidazole ligands functionalized with varying lengths of alkyl groups for antibacterial therapy through multiple modes of action.

In the present study, we have designed and synthesized a series of cationic AIE-active Ir(III) complexes **(Ir1–Ir5)** of cyclometalating 2-phenylbenzimidazole derivatives and NN donor 2,2′-bipyridine ligands as antibacterial theranostic agents (Scheme 1). A selective detection of Gram-positive bacteria by the complexes was observed by fluorescence microscopy imaging, exhibiting strong red emission, corroborating complex-mediated bacterial cell aggregation. The complexes **Ir2–Ir4** displayed efficient antibacterial activity against Gram-positive methicillin-sensitive *S. aureus* (MSSA), methicillin-resistant *S. aureus* (MRSA), *E. faecium*, and *E. faecalis* with minimum inhibitory concentrations (MICs) values in the lower micromolar range of 1–9 μM. Whereas, these complexes were completely inactive towards Gram-negative *E. coli* and *P. aeruginosa* bacteria with >100 μM. The mechanistic investigation of complexes revealed dual modes of action for antibacterial activity *via* membrane depolarization and disruption followed by ROS generation.

Result and Discussion

Design, Synthesis and Characterization of Iridium(III) Complexes (Ir1-Ir5)

In this investigation, a series of cationic cyclometalated iridium(III) complexes (**Ir1-Ir5**) were designed and synthesized to serve as antibacterial theranostic agents. The iridium(III) centers in the complexes were coordinated with two cyclometalating biologically important 2-phenylbenzimidazole ligands and one NN donor 2,2′-bipyridine ligand to achieve an octahedral geometry (Scheme 1). The 2-phenylbenzimidazole ligands in the complexes are attached to alkyl groups of varying chains to provide hydrophobic interaction with alkane chains of the phospholipid layer and pathogenic components, such as lipoteichoic acid (LTA) and lipopolysaccharide (LPS), which are present on the outer cell membranes of Gram-positive and Gram-negative bacteria, respectively. In contrast, 2,2′-bipyridine is conjugated with bis-polyethylene glycol chains for better aqueous solubility and to minimize the cytotoxicity of these complexes.[23,28] The positive charge on the complexes can endow electrostatic interaction with negatively charged bacterial membranes which would help in detection of bacteria.

The benzimidazole ligands (L_2–L_5) derivatized with different alkane chain lengths were synthesized by the reaction of 2-phenylbenzimidazole (L_1) with bromoalkanes.[36] The iridium-dimers $[Ir(L_n)_2Cl]_2$ were synthesized using corresponding benzimidazole ligands ($L_n = L_1$–L_5) with good yields (54–78%). On the other hand, the ancillary **BPy-PEG** ligand was obtained by the coupling of 2,2′-bipyridine dicarboxylic acid with polyethene glycol (PEG_{200}).[23,28] The iridium(III) dimers, $[Ir(L_n)_2Cl]_2$ were reacted with **BPy-PEG** in a mixed solution of DCM-MeOH (2:1,

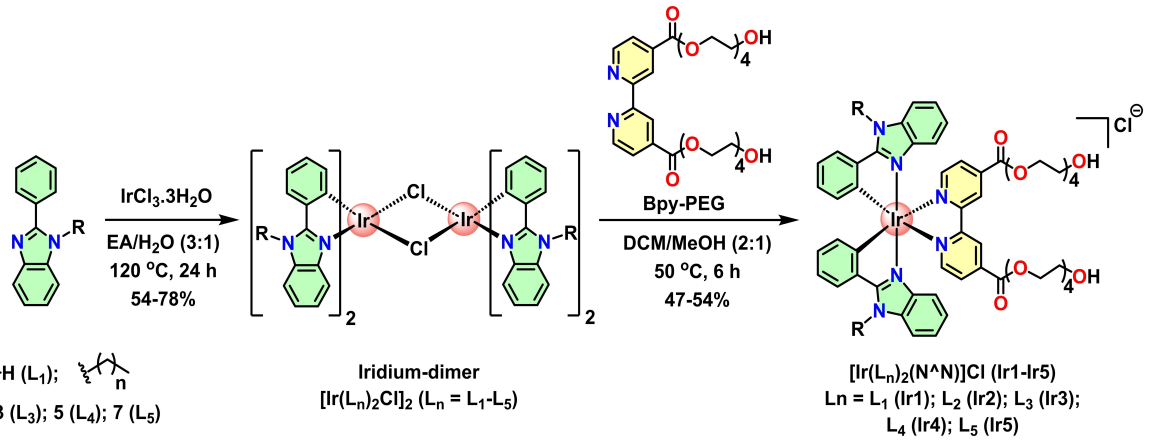

Scheme 1. Synthesis of derivatives of 2-phenylbenzimidazole ligands (L_1-L_5), iridium-dimers ($[Ir(L_n)_2Cl]_2$), and cyclometalated iridium(III) complexes (**Ir1-Ir5**). Here, EA = 2-ethoxyethanol; Bpy-PEG = bipyridine polyethylene glycol.

v/v) at 50 °C to afford corresponding iridium(III) complexes (**Ir1-Ir5**) as illustrated in Scheme 1. The synthesized complexes (**Ir1-Ir5**) were purified by preparative thin layer chromatography and were isolated as chloride salts. The complexes were characterized by NMR, ESI-HRMS, and IR. The complexes were isolated as a mixture of diastereomers. Detailed synthetic procedures and characterization data for the ligands and complexes are provided in the Experimental Section. The complexes showed good solubility in aqueous medium containing 1% DMSO. In the solid state, the FT-IR spectra of the complexes **Ir1-Ir5** showed a strong peak at 1728 cm^{-1} and a strong but broad peak in the range of 3363–3410 cm^{-1} are assignable to stretching vibrations of C=O and -OH groups in the **Bpy-PEG** ligand, respectively. The IR peaks in the range of 700–1585 cm^{-1} are attributed to the presence of aromatic rings. The complexes were structurally characterized by ^{1}H and ^{13}C NMR spectra, and the data are presented in the Experimental Section and in the Supplementary Information (Figures S1–S15). The mass spectral measurements (ESI-HRMS) exhibited a molecular ion peak for the ligands (L_2–L_5) and the complexes (**Ir1–Ir5**) corresponding to their $[M+H]^+$ and $[M-Cl^-]^+$ species, respectively (Figures S16–S24).

Photophysical Properties

The electronic absorption and emission spectra of the complexes (**Ir1–Ir5**) were examined in water containing 0.2% DMSO at 298 K (Figure S25 and Table 1). The complexes exhibited intense absorption bands between 302 and 372 nm, which can be associated to spin-allowed intra-ligand (^{1}IL) $\pi\rightarrow\pi^*$ transitions. On the other hand, the broad and weak absorption bands in the range of 400 to 526 nm could be attributed to ^{1}MLCT and ^{3}MLCT ($d\pi$ (Ir)$\rightarrow\pi^*$) and ^{1,3}LLCT transitions (Figure S25a). These complexes displayed a large Stokes' shifted red emission between 644 and 661 nm upon excitation at 415 nm (Figure S25b and Table 1). Interestingly, upon increasing the length of hydrophobic alkane chains on 2-phenylbenzimidazole ligand in the iridium complexes, the fluorescence signals significantly enhanced. Amongst the complexes studied, complex **Ir5** showed strong fluorescence signals, possibly due to its higher extent of self-aggregation capability due to its presence of longer hydrophobic alkane chain and hydrophilic PEG groups.[23] The absorption and emission maxima and molar extinction coefficients (ε) of the complexes are summarized in Table 1. The quantum yields (Φ) of the complexes were determined to be in the range of 0.014 to 0.050 (Table 1). Moreover, we assessed the lipophilicity of our iridium complexes by measuring their octanol (o) /water (w) partition coefficients ($P_{o/w}=[C]_o/[C]_w$) since lipophilicity plays a significant role in the cellular uptake of drugs. The determined log $P_{o/w}$ values of the complexes were found to be in the range of 1.21 to 1.40 indicating their moderately lipophilic nature (Table 1). Notably, the lipophilicity of these complexes does not seem to significantly affected by the varying length of the alkane chains on 2-phenylbenzimidazole ligands in the complexes.[37]

Determination of AIE Properties of the Iridium(III) Complexes

The AIE properties of the iridium(III) complexes were investigated by measuring emission spectra using fluorescence spectroscopy. Upon excitation at 415 nm, the complexes were weakly emissive in the range of 644–661 nm in aqueous solution, except for **Ir5**. The emission intensity of complexes gradually enhanced with the shift in emission maxima upon the addition of THF fraction from 0 to 98% in the mixed solution (Figures 1a and S26a). The concurrent increase in emission intensity and shifts in emission maxima of the complexes suggest their unique AIE properties.[23,26,28] Next, the aggregation properties of the complexes were confirmed by measuring their hydrodynamic size distribution in absence and presence of THF using dynamic light scattering (DLS) studies (Figures 1 and S26–S27). For example, the hydrodynamic diameters (d) of **Ir2** and **Ir3** in the absence of THF were 59 nm and 79 nm, respectively (Figures 1b and S26b). However, the diameters of **Ir2** and **Ir3** increased significantly to 459 nm and 396 nm, respectively, in the presence of 25% THF in the water – THF mixture (Figures 1c and S26c). Notably, the hydrodynamic diameter of the complexes in water alone is increases with increasing the length of alkane chains on 2-phenylbenzimidazole ligands, suggesting that the aggregation capability of the complexes is influenced by the presence of longer hydrophobic alkane groups (*See* the hydrodynamic diameters in the absence and presence of 25% THF in a water-THF mixture in Figure S27).

Table 1. Physicochemical data of the cyclometalated Ir(III) phenylbenzimidazole complexes (**Ir1-Ir5**).

Complexes	λ_{abs} [a]/nm ($\varepsilon/10^3$ $M^{-1}cm^{-1}$)	λ_{em} [a]/nm	Φ [b]	log $P_{o/w}$ [c]
Ir1	303 (38.4), 370 (10.1), 400 (6.4), 525 (1.1)	660	0.014	1.34
Ir2	304 (35.7), 372 (9.6), 402 (6.3), 525 (1.0)	660	0.034	1.32
Ir3	304 (41.6), 368 (11.2), 400 (7.4), 524 (1.1)	661	0.040	1.31
Ir4	304 (45.4), 370 (12.4), 402 (7.7), 524 (1.3)	645	0.038	1.21
Ir5	302 (42.1), 370 (11.4), 402 (6.8), 526 (1.1)	644	0.050	1.40

[a] Absorption (λ_{abs}) and emission (λ_{em}) spectra of the complexes were investigated in water containing 0.2% DMSO at 298 K. The emission spectra were measured upon excitation at 415 nm. [b] Quantum yields (Φ) were determined in MeCN at 298 K using $[Ru(bpy)_3](PF_6)_2$ ($\Phi=0.0504$) as the reference. [c] Lipophilicity (log $P_{o/w}$) values determined by measuring the partition coefficient of the complexes in n-octanol/water.

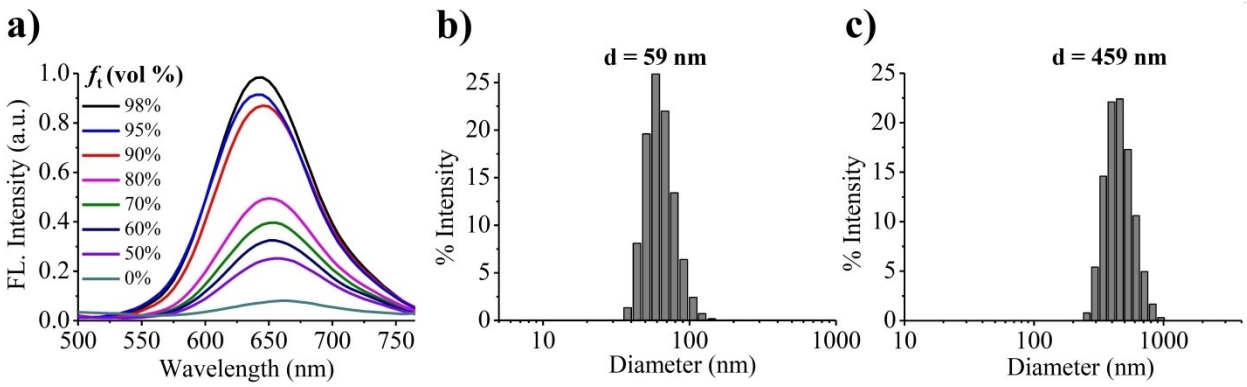

Figure 1. (a) Emission spectra of **Ir2** (50 μM) determined in a water-THF mixture with different THF fractions (f_t). Hydrodynamic diameter (d) and particle size distribution of **Ir2** (50 μM) (b) in the absence and (c) in the presence of 25% THF in a water-THF mixture.

Bacteria Imaging

The AIE properties of the complexes were utilized for imaging of bacteria. In order to determine the intracellular localization of the complexes in bacteria, we have used DNA staining Hoechst dye. For this, Gram-positive MSSA and Gram-negative *E. coli* bacteria were incubated with 10 μM of complex **Ir2**, followed by Hoechst dye (2 μM) and then observed under confocal fluorescence microscope (Figure 2). The imaging results revealed the selective staining of Gram-positive MSSA bacteria, showing a strong red emission of cells treated with **Ir2**, indicating that complex-induced Gram-positive *S. aureus* bacterial aggregation (Figure 2B). An overlay image of **Ir2** and Hoechst indicates that DNA is the major target of the complex (Figure 2D). However, Gram-negative bacterial staining was also observed only at a higher concentration (200 μM) of the complex (Figure S28).

Antimicrobial Activity

The antimicrobial activities of the iridium(III) complexes (**Ir1–Ir5**) were evaluated against the ESKAPE pathogens. Among these, the Gram-positive bacteria *Enterococcus faecium* (*E. faecium*) and methicillin-sensitive *Staphylococcus aureus* (*S. aureus*) (MSSA) and the Gram-negative bacteria *Pseudomonas aeruginosa* (*P. aeruginosa*) were tested. In addition, Gram-positive methicillin-resistant *S. aureus* (MRSA) and *Enterococcus faecalis* (*E. faecalis*) and Gram-negative *Escherichia coli* (*E. coli*) were also examined for clinical interest. Vancomycin (Van) was used as a positive control. The activities of the complexes against these pathogenic bacteria were expressed as minimum inhibitory concentrations (MICs), and compared with clinically approved antibiotic vancomycin (Table 2 and Figures S29–34). The complexes **Ir2–Ir4** exhibited efficient antibacterial activity against Gram-positive bacteria, with low MIC values 1–9 μM, which is comparable to vancomycin and comparable or superior to reported metal complexes.[11,12,16–20,22–25,31–35] In contrast, no activity of these complexes was determined in Gram-negative bacteria (MICs $>$100 μM). This could be attributed to the

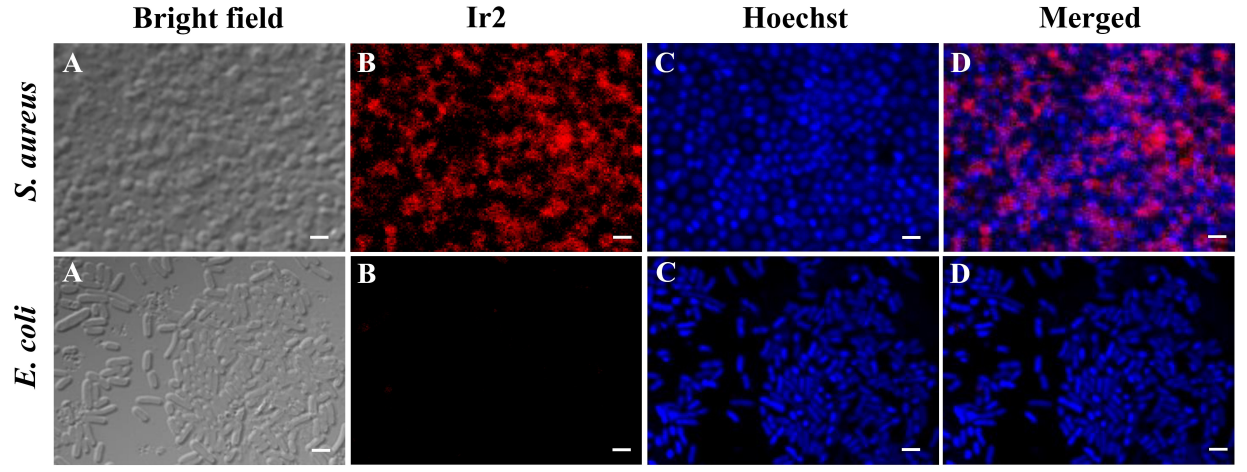

Figure 2. Confocal microscopy images of *S. aureus* and *E. coli* (10^8 CFU/ml) bacterial cells treated with 10 μM of complex **Ir2**. (A) Bright-field image of bacteria, (B) fluorescence image of bacteria treated with **Ir2**, (C) DNA staining with Hoechst dye, and (D) overlay images of B and C. Scale bar: 5 μm.

Table 2. Antibacterial activity against Gram-positive and Gram-negative bacteria and toxicity data in HEK293 cells and human red blood cells of iridium(III) complexes (**Ir1**–**Ir5**).

	Minimum inhibitory concentration (MIC), μM							
	Gram-positive				Gram-negative		Toxicity (μM)	
Compounds	MSSA	MRSA	*E. faecium*	*E. faecalis*	*E. coli*	*Pa*	IC_{50}	HC_{50}
Ir1	14.1	13.1	22.2	14.6	>100	>100	>50	>250
Ir2	1.0	1.0	1.26	1.5	>100	>100	25.2±2.6	>250
Ir3	3.0	4.2	4.5	3.5	>100	>100	28.0±4.0	>250
Ir4	4.7	5.0	8.0	8.8	>100	>100	14.6±2.3	160±12
Ir5	>25	>25	>25	>25	>100	>100	12.9±1.9	172±15
Van	1.7	1.0	1.0	1.0	75	>100	-	-

MSSA = methicillin-sensitive *Staphylococcus aureus*; MRSA = methicillin-resistant *Staphylococcus aureus*; *E. faecium* = *Enterococcus faecium*; *E. faecalis* = *Enterococcus faecalis*; *E. coli* = *Escherichia coli*; Pa = *Pseudomonas aeruginosa*; Van = Vancomycin.

difference in cell wall structures of Gram-positive and Gram-negative bacteria, since the latter contain an extra protective outer membrane, which acts as an effective barrier against antibacterial agents.[18,20,34,38] Nevertheless, dose-dependent cell viability in Gram-positive bacteria was observed that decreases with an increase in complex concentrations. Notably, the antibacterial activity of the complexes decreases with an increase in alkyl chain lengths on cyclometalating 2-phenylbenzimidazole ligands in the complexes. For example, **Ir5** with the longest alkane chain among the series exhibited the lowest antibacterial effect (MIC >25 μM). This may be due to the higher extent of self-aggregation of the complexes with the longer alkyl chains (Figures 1(b,c), S26(b,c) and S27) that could cause their less interaction with bacterial cells, which can potentially decrease their antibacterial properties. Therefore, the extent of bacterial aggregation-induced by the complexes is one of the reasons that could hinder bacterial growth. In contrast, the complex **Ir1** (MIC = 13.1–22.2 μM) with unfunctionalized phenylbenzimidazole ligand displayed lower activity compared to **Ir2**–**Ir4**. The reasons for low activity of **Ir1** have been provided in the following section under mechanistic studies.

Subsequently, in order to classify the complexes as bacteriostatic or bactericidal agents, we investigated the minimum bactericidal concentrations (MBCs) of the complexes in Gram-positive MSSA bacteria (Figure 3). MBC refers to concentrations where no bacterial colonies were observed. The antibacterial agents can be defined as bactericidal agents if the MBC/MIC ratio is ≤4 or bacteriostatic agents if the ratio is >4. MBC values for **Ir1** and **Ir2** in MSSA were determined to be 20 μM and 2.5 μM, respectively. Based on the above results, we concluded that the complexes **Ir1** and **Ir2** exhibit bactericidal activity against MSSA. Vancomycin (Van) also showed a bactericidal mode of cell death in MSSA.

Antibacterial Mechanism

The mechanisms of antibacterial activity of the iridium(III) complexes were investigated in Gram-positive bacteria MSSA. A variety of mechanistic assays were conducted to predict the killing of bacterial cells by these complexes. For mechanistic studies, we have chosen the complexes **Ir1** and **Ir2** containing unsubstituted and alkyl functionalized 2-phenylbenzimidazole ligands, respectively. The cytoplasmic membrane depolarization was monitored using a membrane voltage-sensitive fluorescent dye $DiSC_3(5)$. This cationic dye accumulates in a healthy polarized bacterial cell and leads to its fluorescence quenching. After bacterial membrane disintegration due to stress-induced depolarization, the dye can diffuse back to the media, recovering its fluorescence at 670 nm.[23,25] The results showed that the cells treated with dye exhibited initial fluorescence quenching, however, upon addition of **Ir2** showed a sharp increase in fluorescence intensity compared to control (Figure 4a). In contrast, the enhancement of fluorescence signals was enormously less with the addition of **Ir1**. These results suggest that **Ir2** can depolarize the bacterial cell membrane more efficiently compared to **Ir1**. This result is consistent with our antibacterial activity data presented in Table 2.

Next, the cytoplasmic membrane permeabilization was studied by monitoring the fluorescence intensity of propidium iodide (PI) dye. The PI cannot be internalized in bacterial cells if its membrane is not permeabilized/compromised, resulting in no fluorescent enhancement of this dye being observed. However, this dye can enter into the cytosol of bacteria once the cell membrane of bacteria is permeabilized and then fluoresces at 617 nm upon binding to DNA.[23,35] Thus, the change in bacterial cell membrane permeability by our complexes can be measured by determining PI fluorescence signals. It was found that the fluorescence intensity of PI was remarkably enhanced in **Ir2** than **Ir1**, suggesting greater membrane permeability by the former (Figure 4b). The finding is also supported by the iridium complexes of unsubstituted 2-phenylbenzimidazole ligands displayed antibacterial activity without affecting the cell walls and membranes of bacteria but through ROS generation as reported by Ruiz *et al.*[35]

In order to evaluate whether ROS is involved in killing bacterial cells, a dichlorofluorescein diacetate (DCFH-DA) assay was performed. DCFH-DA is a cell-permeable nonfluorescent dye that after oxidation converted to fluorescent dichlorofluor-

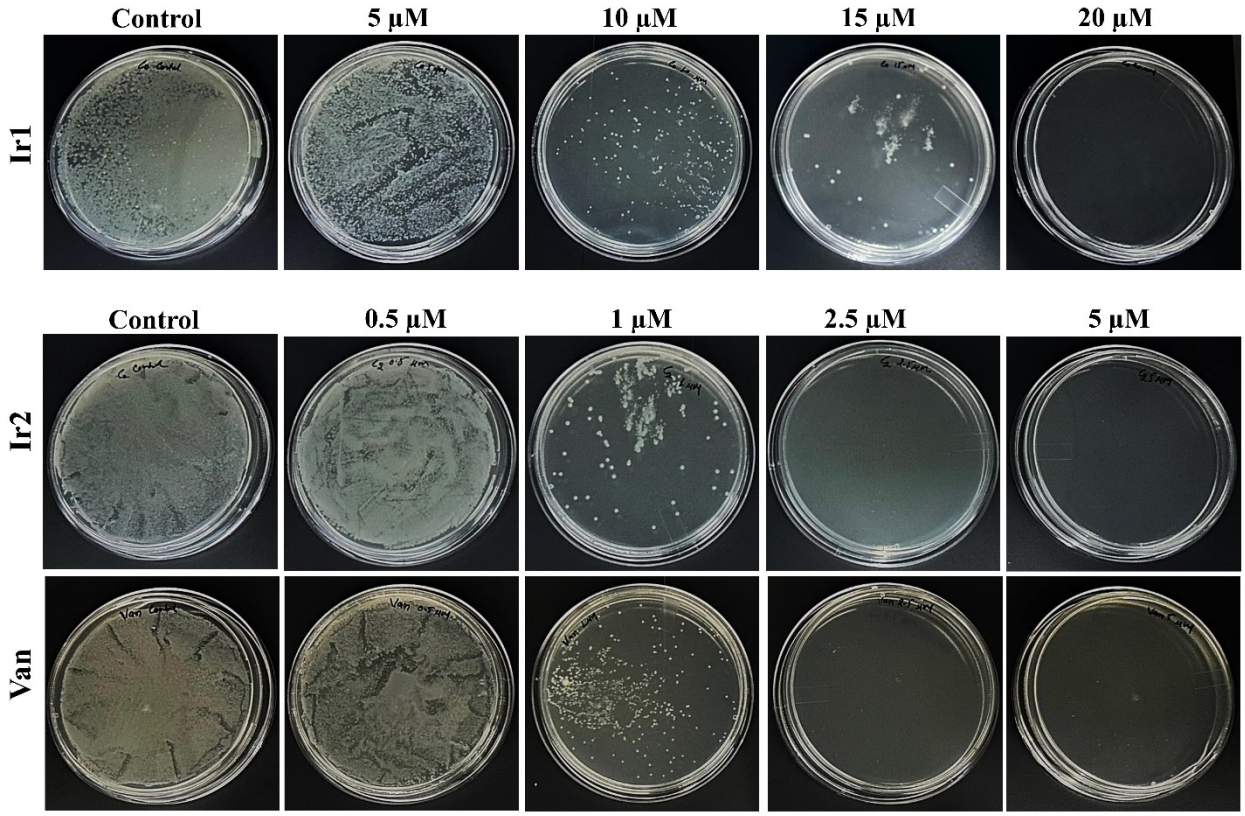

Figure 3. Photographs of colonies of *S. aureus* on agar plates incubated with different concentrations of complexes (**Ir1** and **Ir2**) and vancomycin (Van).

escein (DCF), whose fluorescence is measured at 528 nm.[23,39] The fluorescence intensity of DCF is proportional to the concentration of ROS. Accordingly, MSSA treated with DCFH-DA, followed by incubation with **Ir1** and **Ir2** for different time points. Our results revealed that the fluorescence intensity of DCF enhanced over time in comparison to control, confirming ROS generation (Figure 4c). Notably, the fluorescence intensity of **Ir2** was greater than **Ir1**, indicating the former had greater antibacterial activity than the latter one, which is also good agreement with our antibacterial results (Table 2). Hence, our antibacterial mechanisms indicate that **Ir1** with an unsubstituted 2-phenylbenzimidazole ligand is inefficient in depolarizing and permeabilizing the cell membrane, and even in producing high levels of ROS compared to **Ir2** functionalized with an alkyl group in the phenylbenzimidazole ligand. We hypothesize that these iridium(III) complexes produce ROS through a Fenton-like reaction.[40–42] Furthermore, the events of bacterial killing mechanisms in these complexes suggest that membrane depolarization and membrane permeabilization occur prior to ROS generation (Figure 4).

Further, the antibacterial mechanism of the iridium complexes was investigated by transmission electron microscopy (TEM) analysis to observe the change in bacterial morphology. For this, we recorded the change in morphology of MRSA with and without treatment of complex **Ir2**. Without treatment of complex, bacteria showed smooth and intact spherical shape (Figure 5a,c). However, upon treatment with **Ir2**, the bacteria lost their original shape and the bacterial membrane ruptured.[24] The damage to bacterial cell membrane (shown by yellow arrows in Figure 5b,d) revealed the antibacterial effect of **Ir2**.

Hemolytic Activity and Cytotoxicity

To evaluate the selectivity of the iridium complexes towards bacterial cells, we have accessed hemolytic activity (HC_{50}) and cytotoxicity (IC_{50}) in human red blood cells (RBC) and human embryonic kidney cells (HEK293), respectively (Table 2, Figures 6 and S35). The complexes **Ir4** (HC_{50}, 160 (±15) μM) and **Ir5** (HC_{50}, 172 (±15) μM) exhibited lower hemolytic activity, while **Ir1**–**Ir3** (HC_{50}, >250 μM) did not show hemolytic activity (Figure 6). Interestingly, it was observed that the complexes having longer alkane chains on 2-phenylbenzimidazole ligands (*e.g.*, **Ir4** and **Ir5**) showed slight hemolytic activity. Similarly, the **Ir1** was found to be non-toxic in HEK293 cells (IC_{50} >50 μM), while the cytotoxicity of **Ir2** and **Ir3** were 25.2 and 28.0 μM, respectively, which is ~25 and 7 times of their MIC values. On the other hand, **Ir4** is relatively toxic towards mammalian cells and its cytotoxicity (IC_{50} = 14.6 μM) is ~2–3 times the MICs (4.7–8.8 μM), whereas, **Ir5** (MIC >25 μM) was found to be toxic towards mammalian cells (IC_{50} = 12.9 μM). Notably, the selectivity of these complexes decreases against bacterial cells upon conjugation of longer alkane chains on phenylbenzimidazole ligands (Figure S35). Thus, our combined hemolytic and

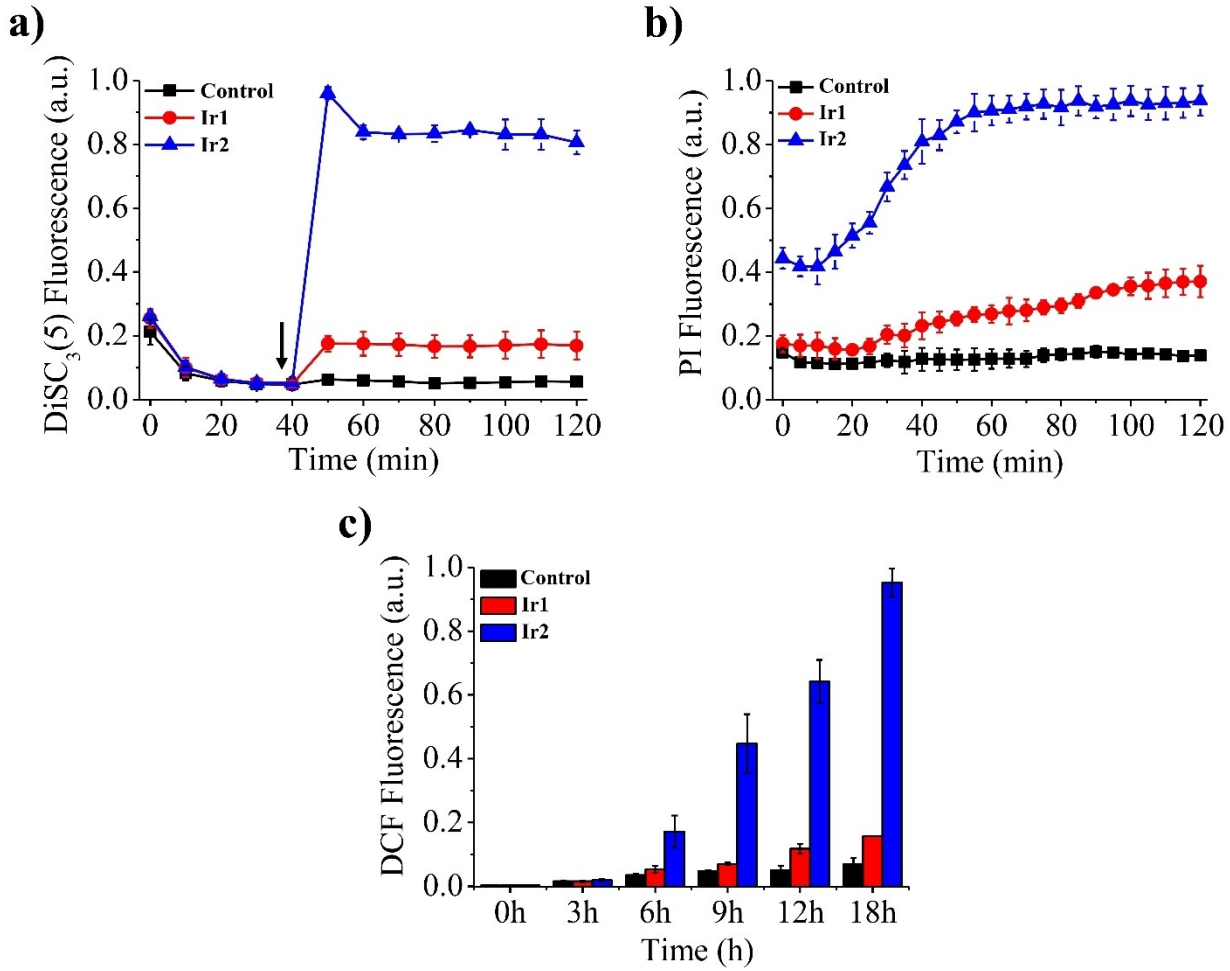

Figure 4. (a) Estimation of membrane depolarization, (b) membrane permeabilization and (c) ROS production of MSSA treated with the complexes **Ir1** (25 μM) and **Ir2** (10 μM) at different time intervals using $DiSC_3(5)$, PI and DCFH-DA dyes, respectively. The arrow in graph (a) indicate the addition of complexes at that point. The black, red and blue symbols and bars represent control (no complex), **Ir1** and **Ir2**, respectively.

cytotoxicity results suggest that the complexes **Ir1–Ir3** exhibit good biocompatibility with mammalian cells.

Conclusions

In summary, in this work, we have designed and synthesized a series of cationic AIE-active iridium(III) complexes (**Ir1–Ir5**) derived from cyclometalating 2-phenylbenzimidazole derivatives and NN donor 2,2′-bipyridine ligands for imaging and killing of bacteria. The complexes can selectively stain Gram-positive bacteria, showing strong red emission of the Ir(III) complexes in the bacteria, indicating complex-mediated aggregation of bacterial cells. The complexes **Ir2-Ir4** exhibited potent antibacterial activity against Gram-positive methicillin-sensitive *S. aureus* (MSSA), methicillin-resistant *S. aureus* (MRSA), *Enterococcus faecium* (*E. faecium*) and *Enterococcus faecalis* (*E. faecalis*), with low MIC values of 1–9 μM. Whereas, the complexes were completely inactive against Gram-negative bacteria *Pseudomonas aeruginosa* (*P. aeruginosa*) and *Escherichia coli* (*E. coli*) upto the tested concentration of 100 μM. The antibacterial effect of these complexes is comparable to clinically approved antibiotic vancomycin (Van) and better than many reported metal complexes. Interestingly, the antibacterial activity of these complexes decreases with the increase in the length of the alkyl chains on 2-phenylbenzimidazole ligands in the complexes. Among these, **Ir2** was found as a best candidate due to its high antibacterial activity (MIC ~1 μM) and non-toxic towards human red blood cells and healthy human embryonic kidney cells (HEK293). The mechanistic investigation suggested dual mode of action of killing bacterial cell *via* loss of membrane integrity followed by ROS.

Experimental Section

Materials

All commercially available solvents were purchased of analytical grade and further dried under argon atmosphere before its use. 2-Phenylbenzimidazole, 2,2′-bipyridine-4,4′-dicarboxylic acid, poly(ethylene glycol) (PEG_{200}), triethylamine, dichlorofluorescein diacetate (DCFH-DA), 3,3′-dipropylthiadicarbocyanine iodide

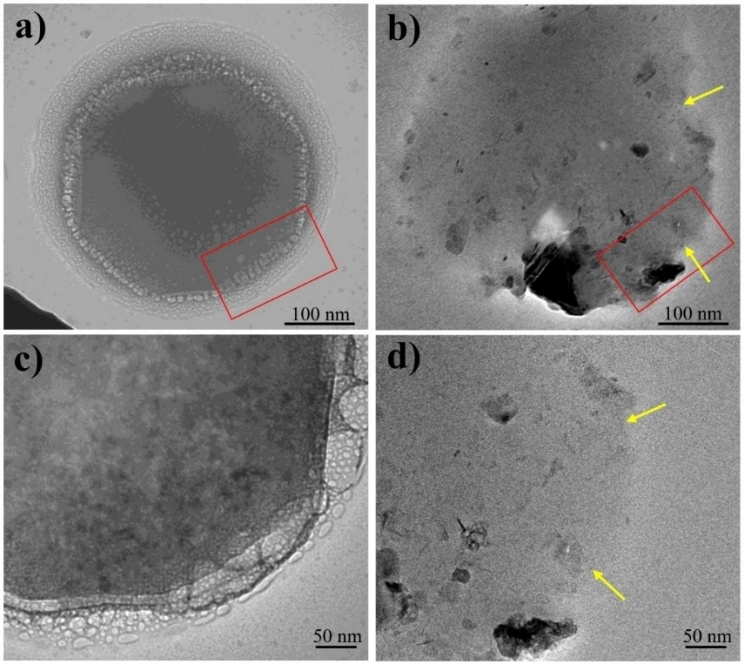

Figure 5. TEM images of MRSA (a and c) without any treatment and (b and d) with treatment of **Ir2** (10 μM) at 30 min. (c) and (d) are enlarged images of the red rectangles in (a) and (b), respectively.

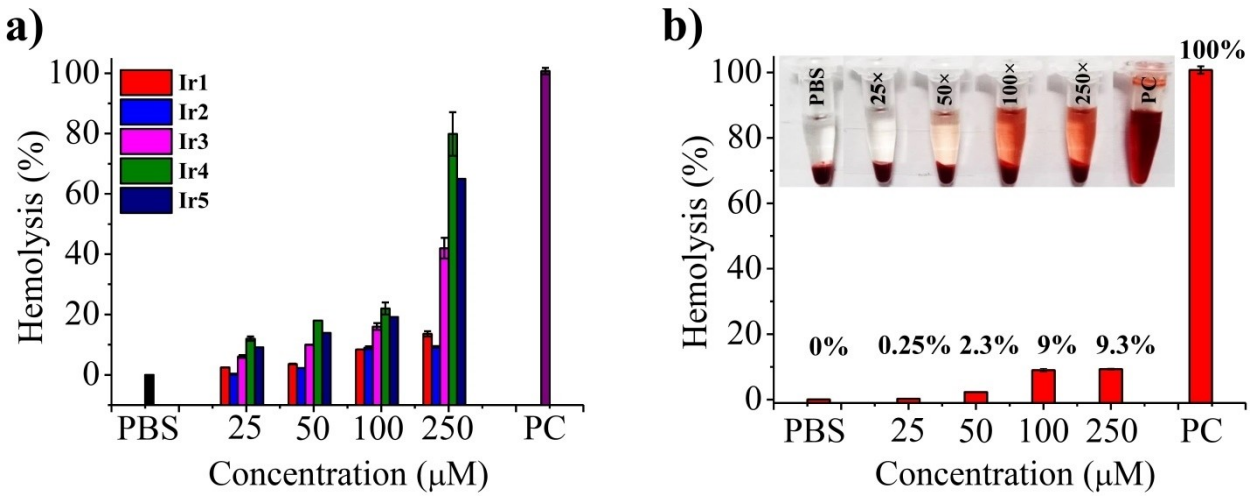

Figure 6. (a) Hemolytic activity of complexes (**Ir1**–**Ir5**) in human red blood cells (RBCs) at different concentrations. (b) Photographs in the inset and quantitative hemolysis of RBCs by **Ir2** at different concentrations (25x, 50x, 100x and 250x of MIC). Here, PC = Positive control (Triton X-100) and PBS as the negative control.

($DiSC_3(5)$), bovine serum albumin (BSA), propidium iodide (PI) and Triton X-100 were purchased from Sigma-Aldrich. $IrCl_3{\cdot}3H_2O$, potassium carbonate and bromoalkanes were obtained from Alfa-Aesar. 1-Ethyl-3-(3 dimethylaminopropyl)carbodiimide (EDC), 1-hydroxybenzotriazole hydrate (HOBt) and glutaraldehyde were procured from Central Drug House (CDH). Thin layer chromatography (TLC) was sourced from Merck, Germany. Nutrient broth and Luria Bertani agar, and vancomycin (Van) hydrochloride obtained from HiMedia. Trypsin, Dulbecco's modified Eagle medium (DMEM), Dulbecco's phosphate-buffered saline (PBS), fetal bovine serum (FBS), 3-(4, 5-dimethylthiazol-2-yl)-2, 5-diphenyltetrazolium bromide (MTT), and penicillin streptomycin solution (pen-strep) were procured from Thermo Fischer Scientific. Hoechst 33342 were sourced from Invitrogen. Bacterial strains methicillin-sensitive *S. aureus* (MTCC 96) and methicillin-resistant *S. aureus* (MTCC 96) were obtained from Amity University, Noida and *E. faecium*, *E. faecalis*, *E. coli* (MTCC 1302) and *P. aeruginosa* (ADK-5) were obtained from All India Institute of Medical Sciences (AIIMS), New Delhi. Human embryonic kidney cells (HEK293) were procured from Cell Repository, NCCS, Pune. Double distilled water and Milli-Q water (~ 18.8 mΩ.cm resistivity) (CDUFBI001, Millipore, USA) were used for the preparation of all the aqueous solutions. The NN donor bipyridine polyethylene glycol (**Bpy-PEG**) ligand was synthesized according to a method reported in the literature.[23,28] The purity of the synthesized iridium(III) complexes (**Ir1-Ir5)** used for biological

evaluation was found to be ≥95% by NMR and high resolution MS spectra.

Measurements

TLC was performed on aluminium plates coated with silica gel mixed with fluorescent indicator. The purification of synthesized ligand and complexes were accomplished using 60–120 mesh silica gel column chromatography. ^{1}H and ^{13}C NMR spectra were acquired on a Bruker 400 and 500 MHz spectrometers in $CDCl_3$ or DMSO-d_6 at ambient temperature with tetramethylsilane (TMS) as an internal standard. NMR standards used were as follows: (^{1}H-NMR) $CDCl_3$ = 7.260 ppm; DMSO-d_6 = 2.50 ppm. (^{13}C-NMR) $CDCl_3$ = 77.00 ppm; DMSO-d_6 = 39.520 ppm. All chemical shifts (δ) are reported in ppm relative to TMS. Spin multiplicities were reported as a singlet (s), doublet (d), triplet (t), quartet (q), doublet of doublets (dd), multiplet (m) and broad (br) with coupling constant (J) reported in Hz. Electrospray ionization high resolution mass spectra (ESI-HRMS) were obtained using a Waters make ESI-MS model synapt G2 high definition mass spectrometry. Fourier transform-Infrared (FT-IR) spectra were measured using IR Affinity-1S (Shimadzu, Kyoto, Japan) FT-IR spectrophotometer equipped with a single reflection attenuated total reflectance (ATR) accessory. The IR spectra were recorded from 4000 to 450 cm^{-1} using a resolution of 4 cm^{-1} with 45 scans. In IR absorption spectra, the shapes and signal intensities (height) of peaks (bands) are denoted by the following abbreviations: br = broad, vs = very strong, s = strong, m = medium and w = weak. UV-vis absorption spectra were recorded using a SpectraMax M2 plate reader (Molecular Devices) and an Agilent Technologies Carry 100 spectrophotometer, respectively, at 298 K from 800 to 200 nm. Emission spectra and quantum yields were measured on Edinburgh Instruments F900 fluorescence spectrophotometer. Dynamic light scattering (DLS) was carried out using Zetasizer Nano ZS90 (Malvern Instrument Ltd., Worcestershire, UK). Transmission electron microscopy (TEM) images were taken on a JEOL JEM-1400 electron microscope operated at an acceleration voltage of 200 kV.

General Procedure for the Synthesis of L_2-L_5[36]

2-Phenylbenzimidazole (50 mg, 0.257 mmol) and potassium carbonate (71.1 mg, 0.514 mmol) were suspended in DMF (1 mL) in an oven-dried round bottom-flask under argon atmosphere and stirred for 30 min at room temperature. To the above mixture, bromoalkane (1.2 equivalents) was added in a dropwise manner over a period of 10 min and then the resulting mixture was heated at 65 °C for 18 h. Thereafter, the mixture was cooled at room temperature and followed by diluted with dichloromethane (15 mL) then washed with water (3x15 mL). The combined organic phase was washed with brine and dried over Na_2SO_4. The organic phase was evaporated on a rotary evaporator to give a pale yellowish oily crude material. The crude material was purified by column chromatography on silica gel using hexane/EtOAc (5:1, v/v) as the eluent to yield a colorless oily product.

L_2 (Yield: 33.1 mg, 58%)

^{1}H-NMR (500 MHz, $CDCl_3$): δ (ppm) 7.84 (m, 1H), 7.73 (m, 2H), 7.52 (m, 3H), 7.44 (m, 1H), 7.32 (m, 2H), 4.29 (q, J = 7.3 Hz, 2H), 1.48 (t, J = 7.3 Hz, 3H). ESI-HRMS (*m/z*) Calcd for $C_{15}H_{14}N_2$ $[M+H]^+$: 223.1230, found: 223.1159.

L_3 (Yield: 40.5 mg, 63%)

^{1}H-NMR (500 MHz, $CDCl_3$): δ (ppm) 7.83 (m, 1H), 7.72 (m, 2H), 7.52 (d, J = 5.8 Hz, 3H), 7.42 (m, 1H), 7.31 (m, 2H), 4.23 (t, J = 7.6 Hz, 2H), 1.80 (m, 2H), 1.28 (m, 2H), 0.86 (t, J = 7.4 Hz, 3H). ESI-HRMS (*m/z*) Calcd for $C_{17}H_{18}N_2$ $[M+H]^+$: 251.1543, found: 251.1472.

L_4 (Yield: 51.4 mg, 72%)

^{1}H-NMR (500 MHz, $CDCl_3$): δ (ppm) 7.83 (m, 1H), 7.71 (m, 2H), 7.52 (m, 3H), 7.42 (m, 1H), 7.31 (m, 2H), 4.22 (t, J = 7.6 Hz, 2H), 1.82 (m, 2H), 1.25–1.20 (m, 6H), 0.83 (t, J = 6.9 Hz, 3H). ^{13}C-NMR (125 MHz, $CDCl_3$): δ (ppm) 153.83, 143.20, 135.68, 130.80, 129.79, 129.45, 128.80, 122.75, 122.42, 120.07, 110.22, 44.82, 31.25, 29.82, 26.46, 22.56, 14.02. ESI-HRMS (*m/z*) Calcd for $C_{19}H_{22}N_2$ $[M+H]^+$: 279.1856, found: 279.1768.

L_5 (Yield: 53.5 mg, 68%)

^{1}H NMR (400 MHz, $CDCl_3$): δ (ppm) 7.83 (m, 1H), 7.71 (m, 2H), 7.52 (m, 3H), 7.42 (m, 1H), 7.31 (m, 2H), 4.22 (m, J = 7.7 Hz, 2H), 1.82 (m, 2H), 1.23 (m, 10H), 0.86 (t, J = 7.0 Hz, 3H). ESI-HRMS (*m/z*) Calcd for $C_{21}H_{26}N_2$ $[M+H]^+$: 307.2169, found: 307.2121.

General Procedure for the Synthesis of Iridium(III) Dimers ($[Ir(L_n)_2Cl]_2$)

An oven dried round bottom flask was charged with $IrCl_3{\cdot}3H_2O$ (30 mg, 0.100 mmol) and the corresponding cyclometalating CN ligand (L_n, 2.2 equivalent). To this, degassed 2-ethoxyethanol/deionized water (2 mL; 3:1 v/v) was introduced under argon atmosphere and the resulting mixture was heated to reflux at 120 °C for 24 h. Thereafter, the mixture was cooled to room temperature, and 4 mL water was added to this and further the mixture was stirred for 1 h to obtain colored precipitates. The precipitate was filtered and washed with deionized water (3x15 mL) and ethanol/water (1:1), then dried under high vacuum to afford corresponding dimers. Due to solubility issues, the dimers $[Ir(L_1)_2Cl]_2$ (Yield: 44 mg, 71%) and $[Ir(L_2)_2Cl]_2$ (Yield: 50 mg, 74%) were proceeded to the next step without characterization.

$[Ir(L_3)_2Cl]_2$ (Yield: 57 mg, 78%)

^{1}H-NMR (400 MHz, $CDCl_3$): δ (ppm) 8.39 (d, J = 8.2 Hz, 1H), 7.48 (d, J = 7.9 Hz, 1H), 7.00 (d, J = 8.0 Hz, 1H), 6.92 (m, 1H), 6.71 (m, 1H), 6.57 (m, 1H), 6.38 (t, J = 7.0 Hz, 1H), 6.01 (d, J = 7.0 Hz, 1H), 4.53 (m, 2H), 2.06 (m, 2H), 1.61 (m, 2H), 1.09 (t, J = 7.4 Hz, 3H).

$[Ir(L_4)_2Cl]_2$ (Yield: 42 mg, 54%)

^{1}H-NMR (500 MHz, $CDCl_3$): δ (ppm) 8.38 (d, J = 8.2 Hz, 1H), 7.47 (d, J = 7.7 Hz, 1H), 6.99 (d, J = 8.2 Hz, 1H), 6.92 (t, J = 7.6 Hz, 1H), 6.71 (t, J = 7.3 Hz, 1H), 6.57 (t, J = 7.6 Hz, 1H), 6.38 (t, J = 7.5 Hz, 1H), 6.02 (d, J = 7.7 Hz, 1H), 4.52 (m, 2H), 2.07 (m, 2H), 1.59 (m, 2H), 1.48–1.38 (m, 4H), 0.95 (t, J = 7.1 Hz, 3H).

$[Ir(L_5)_2Cl]_2$ (Yield: 50 mg, 59%)

^{1}H-NMR (400 MHz, $CDCl_3$): δ (ppm) 8.39 (d, J = 8.2 Hz, 1H), 7.47 (d, J = 7.6 Hz, 1H), 6.99 (d, J = 8.1 Hz, 1H), 6.92 (t, J = 7.3 Hz, 1H), 6.71 (t, J = 7.0 Hz, 1H), 6.57 (t, J = 7.3 Hz, 1H), 6.39 (t, J = 7.1 Hz, 1H), 6.02 (d, J = 7.9 Hz, 1H), 4.52 (m, 2H), 2.07 (m, 2H), 1.60 – 1.33 (m, 10H), 0.91 (t, J = 6.8 Hz, 3H).

Synthesis of Ir1

A mixture of iridium(III) dimer ($[Ir(L_1)_2Cl]_2$: 24.5 mg, 0.020 mmol) and NN donor ligand (**Bpy-PEG**: 26.7 mg, 0.044 mmol) was heated in a 25 mL oven-dried round bottom-flask sealed with a rubber septum containing a mixed solution of CH_2Cl_2/MeOH (2:1, v/v, 2.5 mL) at 50 °C under argon atmosphere for 6 h. Subsequently, the solution was cooled to room temperature, and solvent was removed on a rotary evaporator. The resulting solid was washed with hexane (3x15 mL). The crude material was purified by preparative thin layer chromatography using CH_2Cl_2/MeOH (20:1, v/v). The product was dried under vacuum to afford **Ir1** (Yield: 22.7 mg, 47%).

^{1}H-NMR (500 MHz, DMSO-d_6): δ (ppm) 9.24 (m, 2H), 8.36 (m, 1H), 8.18 (m, 2H), 7.97 (d, J = 7.5 Hz, 2H), 7.79 (m, 1H), 7.61 (m, 3H), 7.41 (d, J = 7.6 Hz, 1H), 7.22 (m, 2H), 7.05 (t, J = 7.4 Hz, 2H), 6.93 (m, 2H), 6.85 (t, J = 7.2 Hz, 2H), 6.20 (d, J = 7.3 Hz, 1H), 5.71 (m, 1H), 4.49 (m, 4H), 3.81 (m, 4H), 3.72–3.37 (m, 24H). ^{13}C-NMR (125 MHz, $CDCl_3$): δ (ppm) 163.96, 163.25, 156.88, 152.25, 149.51, 139.53, 139.39, 139.19, 133.98, 133.27, 132.44, 130.60, 128.01, 124.51, 123.91, 123.83, 123.38, 122.49, 122.38, 113.17, 72.38, 72.33, 72.31, 72.29, 69.77, 68.05, 65.54, 60.21. IR (ATR) ν (cm^{-1}): 3394 br (O–H), 2922 m (C–H: aliphatic), 1728 vs (C=O), 1593 m, 1537 m, 1467 m, 1454 m, 1406 w, 1257 s, 1232 s, 1101 s, 1022 s, 819 w, 738 vs, 702 w. ESI-HRMS (*m/z*) Calcd for $C_{54}H_{58}IrN_6O_{12}^+$ $[M–Cl^-]^+$: 1175.3736, found: 1175.3588.

Synthesis of Ir2

This complex was synthesized in an identical manner to that described for **Ir1**, using a mixture of $[Ir(L_2)_2Cl]_2$ (26.8 mg, 0.020 mmol) and **Bpy-PEG** (26.7 mg, 0.044 mmol). Yield: 24.8 mg, 49%.

^{1}H-NMR (500 MHz, $CDCl_3$): δ (ppm) 9.12 (s, 2H), 8.34 (d, J = 5.6 Hz, 2H), 8.07 (dd, J = 5.6, 1.5 Hz, 2H), 7.82 (d, J = 7.9 Hz, 2H), 7.53 (d, J = 8.3 Hz, 2H), 7.30 (t, J = 7.5 Hz, 2H), 7.11 (m, 2H), 6.92 (t, J = 7.8 Hz, 2H), 6.86 (m, 2H), 6.28 (d, J = 7.6 Hz, 2H), 5.63 (d, J = 8.3 Hz, 2H), 4.81 (m, 4H), 4.06 (m, 8H), 3.74–3.59 (m, 23H), 1.65 (t, J = 7.3 Hz, 6H). IR (ATR) ν (cm^{-1}): 3363 br (O–H), 2920 m (C–H: aliphatic), 1728 vs (C=O), 1583 w, 1506 m, 1479 w, 1433 s, 1261 s, 1236 s, 1195 m, 1105 s, 742 vs, 702 m. ESI-HRMS (*m/z*) Calcd for $C_{58}H_{66}IrN_6O_{12}^+$ $[M–Cl^-]^+$: 1231.4362, found: 1231.5392.

Synthesis of Ir3

This complex was synthesized in an identical manner to that described for **Ir1**, using a mixture of $[Ir(L_3)_2Cl]_2$ (29 mg, 0.020 mmol) and **Bpy-PEG** (26.7 mg, 0.044 mmol). Yield: 25.9 mg, 49%.

^{1}H-NMR (400 MHz, $CDCl_3$): δ (ppm) 9.24 (m, 1H), 8.89 (m, 1H), 8.31 (m, 2H), 8.03 (m, 2H), 7.78 (d, J = 7.6 Hz, 2H), 7.48 (m, 2H), 7.30 (m, 2H), 7.09 (m, 2H), 6.94 (m, 2H), 6.84 (t, J = 7.4 Hz, 2H), 6.27 (m, 2H), 5.64 (m, 2H), 4.75–4.50 (m, 8H), 3.99 (m, 4H), 3.75–3.47 (m, 24H), 2.0 (m, 4H), 1.50 (m, 4H), 1.00 (t, J = 7.3 Hz, 6H). IR (ATR) ν (cm^{-1}): 3405 br (O–H), 2927 m (C–H: aliphatic), 1728 vs (C=O), 1583 w, 1556 w, 1406 m, 1361 m, 1255 s, 1234 m, 928 m, 759 m, 721 s. ESI-HRMS (*m/z*) Calcd for $C_{62}H_{74}IrN_6O_{12}^+$ $[M–Cl^-]^+$: 1287.4988, found: 1287.2275.

Synthesis of Ir4

This complex was synthesized in an identical manner to that described for **Ir1**, using a mixture of $[Ir(L_4)_2Cl]_2$ (31.3 mg, 0.020 mmol) and **Bpy-PEG** (26.7 mg, 0.044 mmol). Yield: 28 mg, 51%.

^{1}H-NMR (500 MHz, $CDCl_3$): δ (ppm) 9.20 (s, 2H), 8.32 (d, J = 5.6 Hz, 2H), 8.06 (dd, J = 5.6, 1.5 Hz, 2H), 7.78 (d, J = 7.8 Hz, 2H), 7.48 (d, J = 8.3 Hz, 2H), 7.29 (m, 1H), 7.10 (m, 1H), 6.92 (t, J = 7.8 Hz, 2H), 6.85 (t, J = 7.1 Hz, 2H), 6.27 (d, J = 7.0 Hz, 2H), 5.62 (d, J = 8.2 Hz, 2H), 4.69 (m, 4H), 4.07 (m, 8H), 3.75–3.60 (m, 21H), 2.01 (m, 4H), 1.32 (m, 12H), 0.88 (d, J = 7.1 Hz, 6H). IR (ATR) ν (cm^{-1}): 3392 br (O–H), 2923 m (C–H: aliphatic), 1728 vs (C=O), 1629 w, 1583 w, 1502 m, 1404 w, 1259 s, 1068 s, 1031 m, 742 vs, 702 m. ESI-HRMS (*m/z*) Calcd for $C_{66}H_{82}IrN_6O_{12}^+$ $[M–Cl^-]^+$: 1343.5614, found: 1343.6488.

Synthesis of Ir5

This complex was synthesized in an identical manner to that described for **Ir1**, using a mixture of $[Ir(L_5)_2Cl]_2$ (33.5 mg, 0.020 mmol) and **Bpy-PEG** (26.7 mg, 0.044 mmol). Yield: 31 mg, 54%.

^{1}H-NMR (500 MHz, $CDCl_3$): δ (ppm) 9.16 (m, 1H), 8.91 (m, 1H), 8.31 (m, 2H), 8.09 (m, 2H), 7.77 (t, J = 8.1 Hz, 2H), 7.46 (t, J = 8.2 Hz, 2H), 7.29 (t, J = 6.7 Hz, 2H), 7.09 (m, 2H), 6.92 (m, 2H), 6.84 (t, J = 7.3 Hz, 2H), 6.27 (d, J = 7.3 Hz, 2H), 5.64 (m, 2H), 4.74–4.55 (m, 8H), 4.01 (m, 4H), 3.73–3.51 (m, 25H), 2.01 (m, 4H), 1.50–1.27 (m, 20H), 0.86 (t, J = 7.0 Hz, 6H). ^{13}C-NMR (125 MHz, $CDCl_3$): δ (ppm) 162.33, 157.55, 157.31, 152.45, 138.84, 135.26, 133.63, 133.57, 131.01, 125.22, 125.14, 124.84, 124.76, 124.06, 123.31, 113.68, 113.55, 111.25, 111.16, 73.09, 72.68, 70.66, 70.58, 70.52, 70.09, 61.86, 61.68, 54.01, 45.32, 31.82, 29.82, 29.72, 29.31, 29.24, 26.92, 22.70, 14.20. IR (ATR) ν (cm^{-1}): 3410 br (O–H), 2922 m (C–H: aliphatic) 1728 vs (C=O), 1583 w, 1556 w, 1406 m, 1321 m, 1257 s, 1234 m, 1120 s, 1029 m, 925 w, 723 s, 702 w. ESI-HRMS (*m/z*) Calcd for $C_{70}H_{90}IrN_6O_{12}^+$ $[M–Cl^-]^+$: 1399.6240, found: 1399.5513.

Notably, among the complexes **Ir1-Ir5**, we have provided ^{13}C NMR data for **Ir1** and **Ir5**. The reason for this is that the iridium center in **Ir1** and **Ir5** is coordinated with unsubstituted 2-phenylbenzimidazole and C_8H_{17} alkyl functionalized 2-phenylbenzimidazole ligands, respectively. In **Ir2-Ir5**, 2-phenylbenzimidazole ligands are attached to varying lengths of alkyl groups. In ^{13}C NMR spectra, these alkyl carbons overlap and appear almost with identical chemical shift values. Hence, these alkyl carbons in **Ir2-Ir5** are not clearly distinguished from ^{13}C NMR.

UV-Visible Spectra

The absorption spectra of the iridium(III) complexes **Ir1–Ir5** were determined in water containing 0.2% DMSO at room temperature. All UV-vis spectroscopic measurements were performed in a quartz cuvette with an optical path length of 10 mm. The wavelength was reported in nanometers (nm).

Emission Spectra and Determination of Quantum Yields

Emission spectra of iridium(III) complexes were measured in water containing 0.2% DMSO at room temperature using a quartz cuvette with an optical path length of 10 mm. The excitation wavelength of all the complexes was 415 nm. Quantum yields (Φ) of all the complexes were studied in MeCN at room temperature using $[Ru(bpy)_3](PF_6)_2$ (Φ = 0.0504) as the reference.

Aggregation-Induced Emission Studies[23,26,28]

The iridium complexes (50 μM) were prepared in water containing 1% DMSO in final volume of 2 ml. The complexes were titrated with the different amounts of THF keeping the total volume (water plus THF) constant (2 ml) and measured their phosphorescence emission spectra. The hydrodynamic diameters (d) of the complexes

in water and its aggregated particles in water-THF mixtures were determined by DLS.

Determination of Lipophilicity

The lipophilicity of the iridium(III) complexes were determined by measuring their partition coefficients (log $P_{o/w}$) between n-octanol (o) and water (w) using the classical flask-shaking method.[43,44] Briefly, 0.5 mg of complexes was taken in 3 ml of n-octanol and water mixture (1 : 1, v/v) and mixed vigorously for 24 h. Then the mixture was kept at room temperature in a stationary state for an additional 24 h to reach saturation. After that the n-octanol and water phases were separated. The concentration of complexes was then measured by UV-vis spectroscopy in both the n-octanol (C_o) and water (C_w) phases to determine the log $P_{o/w} = \log [C]_o/[C]_w$, where $[C]_o$ and $[C]_w$ are the concentrations of the complex in the n-octanol and water phases, respectively.

Bacteria Imaging

MSSA and *E. coli* bacteria were grown in their mid-log phase and 10^8 CFU/ml of bacteria were harvested, washed and resuspended in PBS. Then, 10 μM of complex **Ir2** was incubated with 1 ml of bacterial suspension for 30 min at 37 °C, and the unbounded **Ir2** was removed by centrifugation at 3000 rpm for 3 min and the bacterial pellet was resuspend in 500 μl PBS. Subsequently, the bacteria were stained with nucleic acid dye Hoechst (2 μM dissolved in PBS) for 10 min at room temperature. After this the bacteria were washed three times with PBS and the bacterial cells were further resuspended in 100 μl of PBS. Thereafter, 20 μl aliquot of bacterial suspension were dropped onto clean microscopic slides and covered with coverslips for immobilization. Then the stained cells were visualized under Nikon Eclipse Ti–E microscope and Magnus Trinocular MLXi Plus microscope. Hoechst and complex **Ir2** were both excited with 405 nm laser.

Antibacterial Activity Studies

The antibacterial activity (MIC values) of the complexes against various Gram-positive and Gram-negative bacteria were evaluated by the broth microdilution method according to CLSI guidelines.[45] The bacterial strains were cultured in Nutrient broth to achieve 10^8 CFU/ml confluency. To investigate the MIC, the bacterial density was further diluted to 10^5 CFU/ml. Accordingly, the different concentrations of the compounds were prepared in broth. Then the 100 μl media solutions with bacteria were dispensed to each well of 96 plates. Subsequently, 100 μl complex solutions were added to each well of 96 plates to make the final volume of 200 μl. The compound concentrations used in Gram-positive and Gram-negative bacteria in the range of 0.1–50 μM and 1–100 μM, respectively. Then the plates were incubated at 37 °C for 18 h. The MIC values were determined by measuring the absorbance at 600 nm using SpectraMax M2 plate reader (Molecular Devices). The inhibition of bacterial growth was calculated with reference to control having only bacteria without drug treatment. Minimum bactericidal concentrations (MBCs) of the complexes were determined by taking 5 μl volumes of different concentrations of sample solution from the 96-wells and spreading them over agar plates. Next, the agar plates were incubated at 37 °C for 18 h without shaking. The concentration where no visible bacterial colonies were observed in the agar plate corresponded to the MBC. Triplicate wells were used for each concentration, and the experiments were conducted three times.

TEM Imaging of Bacteria[16,28]

A 10^8 CFU/ml bacterial suspension of MRSA was incubated with complex **Ir2** (10 μM) for 30 min at 37 °C. Subsequently, the bacterial suspensions were centrifuged at 4000 rpm for 5 min and washed with PBS (pH 7.4) three times. The bacteria were then fixed with 2.5 % glutaraldehyde in PBS at 4 °C for 4 h. Further, the bacterial suspensions were centrifuged at 2000 rpm for 5 min and washed with PBS two times, and then centrifuged. Thereafter, the bacterial pellet was resuspended in 40 % ethanol and dehydrated with 70, 80 and 90 % ethanol for 30 min each at 4 °C. 10 μl of aliquots from sample were deposited on carbon coated copper grids (CF 200 CU, Electron Microscopy Sciences, USA) and allowed for slow evaporation at room temperature overnight. The dried sample was imaged using a JEOL JEM-1400 electron microscope.

Mechanistic Studies

ROS Quantification Assay

The production of ROS by the complexes was determined using dichlorofluorescein diacetate (DCFH-DA) dye by fluorescence spectroscopy. For this, 10^8 CFU/ml of MSSA were grown in mid-log phase, then harvested, washed and resuspended in fresh broth. The stock solution of the complexes was prepared in broth media. The bacterial suspension (10^8 CFU/ml) was treated with the complexes **Ir1** (25 μM) and **Ir2** (10 μM) in 96 well plates. To this, 5 μl of DCFH-DA was added to reach a final concentration of 5 μM in a total volume of 200 μl. Subsequently, the bacteria in 96 well plates were incubated without shaking at 37 °C and the ROS production was monitored by determining the fluorescence intensity of dichlorofluorescein (DCF) at 528 nm ($\lambda_{ex} = 488$ nm) using SpectraMax M2 plate reader. Bacteria treated with dye alone served as a control.

Cytoplasmic Membrane Depolarization Assay

Cytoplasmic membrane depolarization of bacteria by the complexes were monitored by a membrane voltage-sensitive fluorescent dye $DiSC_3(5)$. Accordingly, 10^8 CFU/ml of MSSA bacteria was grown in mid log phase and then harvested and resuspended in Nutrient broth supplemented with 0.5 mg/ml of BSA. BSA solution was added to the broth to reduce $DiSC_3(5)$ absorption onto the polystyrene surface. The stock solutions of the complexes were prepared in broth media. The bacterial solution was diluted to give 10^7 CFU/ml bacteria. Then 190 μl of bacterial suspension was treated with 5 μl of $DiSC_3(5)$ dye (1 μM final concentration) in 96 well plate. The fluorescence of the dye was monitored using SpectraMax M2 plate reader at 670 nm ($\lambda_{ex} = 610$ nm). At first, the dye was equilibrated with the bacteria to obtain maximum self-quenching (or a minimum steady fluorescence signal). Thereafter, 5 μl of complex was added to each well at a final concentration of 25 and 10 μM for **Ir1** and **Ir2**, respectively, and the fluorescence signal was monitored for 2 h. A control experiment was performed with bacteria suspension treated with dye only.

Cytoplasmic Membrane Permeabilization Assay

A 10^8 CFU/ml of MSSA were grown in mid-log phase and then harvested, washed and resuspended in 1 : 1 ratio of 5 mM glucose and 5 mM HEPES buffer (pH 7.4). The stock solutions of the complexes were prepared in broth media. A 10 μl of complex solution was then added to 165 μl of resuspended bacteria in black nunc 96 well microtitre plates containing 25 μl of 10 μM of propidium iodide (PI). The final concentration of iridium complex was 25 and 10 μM for **Ir1** and **Ir2**, respectively, in this total volume

of 200 μl. The fluorescence intensity of the PI dye was recorded for 2 h at 5 min intervals at an excitation and emission wavelengths of 535 nm and 617 nm, respectively. A control experiment was performed with bacteria suspension treated with dye only.

Toxicity Studies

Hemolysis Assay

The hemolytic activity of the complexes was tested in human red blood cells (RBCs) according to literature report.[11,20] Briefly, 1.5 ml of human blood was collected in K_2EDTA tube from healthy donor and centrifuged at 2000 rpm for 10 min to separate the RBCs from plasma. Then the RBCs pellet was washed three times with 1XPBS (pH 7.4) by centrifuging at 3000 rpm for 3 min. The RBCs pellet was resuspended in 10 ml PBS and then the cells were treated with different concentrations of the complexes and 10% Triton X-100 used as positive control. The RBCs suspension was incubated at 37 °C for 1 h and then the mixture was centrifuged at 2000 rpm for 5 min. The supernatant was transferred to a 96 well plate (100 μl) at its absorbance was determined at 540 nm. The hemolysis (%) was calculated using the following formula:

$$\text{hemolysis } (\%) = [(A - A_0)/(A_{total} - A_0)] \times 100.$$

Where, the absorbance of a well-treated with a complex (A) to that which was not treated (A_0), and the overall response was normalized with respect to the Triton X-treated well (A_{total}) assuming 100% lysis of RBCs.

Cytotoxicity Assay

The cytotoxicity (IC_{50}) of the complexes were evaluated in human embryonic kidney cells (HEK293) by MTT assay. The cells were cultured in DMEM media with 10% FBS and 1% pen-strep at 37 °C in a CO_2 incubator. After 90% confluency, cells were trypsinized, centrifuged and redispersed in complete media. Then the cultured cells were seeded in 96-well plate as triplicate at a density of 9000 cells/well and the plates were kept in a CO_2 incubator for 24 h. The stock solution of the complexes was prepared in complete media. The media from HEK293 cells were removed and added different concentration of complexes from 2.5 to 50 μM in a 200 μl of total volume. The cells were incubated with the complexes for 24 h in a CO_2 incubator. The cells were then washed with PBS followed by addition of 200 μl of DMEM and 20 μl of MTT solution (5 mg ml^{-1} in PBS) to each well and incubated at 37 °C for 3 h. Then the medium was discarded and replaced with 200 μl of DMSO in each well to dissolve the formazan crystals formed. The cell viability was determined by measuring the absorbance at 570 nm using a SpectraMax M2 microtitre plate reader.

Acknowledgements

P. K. S. acknowledges MHRD-STARS (MoE-STARS/STARS-1/374), BRNS (58/14/15/2023-BRNS/12127), and SERB, DST (CRG/2023/005243) for financial support. P. P. acknowledge SERB, DST (SRG/2023/001099) for financial support. A. Gautam and A. Gupta gratefully acknowledge the BRNS and MHRD-STARS, respectively, for fellowships. We thank AIRF, JNU for the instrumentation facilities. AICCRS, Amity University, Uttar Pradesh and AIIMS, New Delhi are acknowledged for providing bacterial strains.

Conflict of Interests

The authors declare no conflict of interest.

Data Availability Statement

The data that support the findings of this study are available from the corresponding author upon reasonable request.

Keywords: Aggregation-induced emission · Antibiotics · Gram-positive bacteria · Iridium · Phenylbenzimidazole

[1] P. Prasad, A. Gupta, P. K. Sasmal, *Chem. Commun.* **2021**, *57*, 174–186.
[2] G. Mancuso, A. Midiri, E. Gerace, C. Biondo, *Pathogens* **2021**, *10*, 1310.
[3] C. J. L. Murray, K. S. Ikuta, F. Sharara, L. Swetschinski, G. Robles Aguilar, A. Gray, C. Han, C. Bisignano, P. Rao, E. Wool, S. C. Johnson, A. J. Browne, M. G. Chipeta, F. Fell, S. Hackett, G. Haines-Woodhouse, B. H. Kashef Hamadani, E. A. P. Kumaran, B. McManigal, S. Achalapong, R. Agarwal, S. Akech, S. Albertson, J. Amuasi, J. Andrews, A. Aravkin, E. Ashley, F.-X. Babin, F. Bailey, S. Baker, B. Basnyat, A. Bekker, R. Bender, J. A. Berkley, A. Bethou, J. Bielicki, S. Boonkasidecha, J. Bukosia, C. Carvalheiro, C. Castañeda-Orjuela, V. Chansamouth, S. Chaurasia, S. Chiurchiù, F. Chowdhury, R. Clotaire Donatien, A. J. Cook, B. Cooper, T. R. Cressey, E. Criollo-Mora, M. Cunningham, S. Darboe, N. P. J. Day, M. De Luca, K. Dokova, A. Dramowski, S. J. Dunachie, T. Duong Bich, T. Eckmanns, D. Eibach, A. Emami, N. Feasey, N. Fisher-Pearson, K. Forrest, C. Garcia, D. Garrett, P. Gastmeier, A. Z. Giref, R. C. Greer, V. Gupta, S. Haller, A. Haselbeck, S. I. Hay, M. Holm, S. Hopkins, Y. Hsia, K. C. Iregbu, J. Jacobs, D. Jarovsky, F. Javanmardi, A. W. J. Jenney, M. Khorana, S. Khusuwan, N. Kissoon, E. Kobeissi, T. Kostyanev, F. Krapp, R. Krumkamp, A. Kumar, H. H. Kyu, C. Lim, K. Lim, D. Limmathurotsakul, M. J. Loftus, M. Lunn, J. Ma, A. Manoharan, F. Marks, J. May, M. Mayxay, N. Mturi, T. Munera-Huertas, P. Musicha, L. A. Musila, M. M. Mussi-Pinhata, R. N. Naidu, T. Nakamura, R. Nanavati, S. Nangia, P. Newton, C. Ngoun, A. Novotney, D. Nwakanma, C. W. Obiero, T. J. Ochoa, A. Olivas-Martinez, P. Olliaro, E. Ooko, E. Ortiz-Brizuela, P. Ounchanum, G. D. Pak, J. L. Paredes, A. Y. Peleg, C. Perrone, T. Phe, K. Phommasone, N. Plakkal, A. Ponce-de-Leon, M. Raad, T. Ramdin, S. Rattanavong, A. Riddell, T. Roberts, J. V. Robotham, A. Roca, V. D. Rosenthal, K. E. Rudd, N. Russell, H. S. Sader, W. Saengchan, J. Schnall, J. A. G. Scott, S. Seekaew, M. Sharland, M. Shivamallappa, J. Sifuentes-Osornio, A. J. Simpson, N. Steenkeste, A. J. Stewardson, T. Stoeva, N. Tasak, A. Thaiprakong, G. Thwaites, C. Tigoi, C. Turner, P. Turner, H. R. van Doorn, S. Velaphi, A. Vongpradith, M. Vongsouvath, H. Vu, T. Walsh, J. L. Walson, S. Waner, T. Wangrangsimakul, P. Wannapinij, T. Wozniak, T. E. M. W. Young Sharma, K. C. Yu, P. Zheng, B. Sartorius, A. D. Lopez, A. Stergachis, C. Moore, C. Dolecek, M. Naghavi, *Global burden of bacterial antimicrobial resistance in 2019: a systematic analysis. Lancet* **2022**, *399*, 629–655.
[4] T. Coque, D. Graham, A. Pruden, A. So, E. Topp, *Bracing for Superbugs: Strengthening environmental action in the One Health response to antimicrobial resistance*, United Nations Environment Programme, Technical report, **2023**.
[5] J. O'Neill, *Antimicrobial resistance: Tackling a crisis for the health and wealth of nations, Rev. Antimicrob. Resist.* **2014**, *20*, 1–16 .
[6] A. Frei, J. Zuegg, A. G. Elliott, M. Baker, S. Braese, C. Brown, F. Chen, C. G. Dowson, G. Dujardin, N. Jung, A. P. King, A. M. Mansour, M. Massi, J. Moat, H. A. Mohamed, A. K. Renfrew, P. J. Rutledge, P. J. Sadler, M. H. Todd, C. E. Willans, J. J. Wilson, M. A. Cooper, M. A. T. Blaskovich, *Chem. Sci.* **2020**, *11*, 2627–2639.
[7] E. Tacconelli, E. Carrara, A. Savoldi, S. Harbarth, M. Mendelson, D. L. Monnet, C. Pulcini, G. Kahlmeter, J. Kluytmans, Y. Carmeli, M. Ouellette, K. Outterson, J. Patel, M. Cavaleri, E. M. Cox, C. R. Houchens, M. L. Grayson, P. Hansen, N. Singh, U. Theuretzbacher, N. Magrini, A. O. Aboderin, S. S. Al-Abri, N. Awang Jalil, N. Benzonana, S. Bhattacharya,

A. J. Brink, F. R. Burkert, O. Cars, G. Cornaglia, O. J. Dyar, A. W. Friedrich, A. C. Gales, S. Gandra, C. G. Giske, D. A. Goff, H. Goossens, T. Gottlieb, M. Guzman Blanco, W. Hryniewicz, D. Kattula, T. Jinks, S. S. Kanj, L. Kerr, M.-P. Kieny, Y. S. Kim, R. S. Kozlov, J. Labarca, R. Laxminarayan, K. Leder, L. Leibovici, G. Levy-Hara, J. Littman, S. Malhotra-Kumar, V. Manchanda, L. Moja, B. Ndoye, A. Pan, D. L. Paterson, M. Paul, H. Qiu, P. Ramon-Pardo, J. Rodríguez-Baño, M. Sanguinetti, S. Sengupta, M. Sharland, M. Si-Mehand, L. L. Silver, W. Song, M. Steinbakk, J. Thomsen, G. E. Thwaites, J. W. M. van der Meer, N. Van Kinh, S. Vega, M. V. Villegas, A. Wechsler-Fördös, H. F. L. Wertheim, E. Wesangula, N. Woodford, F. O. Yilmaz, A. Zorzet, *Lancet Infect. Dis.* **2018**, *18*, 318–327.

[8] N. A. Turner, B. K. Sharma-Kuinkel, S. A. Maskarinec, E. M. Eichenberger, P. P. Shah, M. Carugati, T. L. Holland, V. G. Fowler Jr, *Nat. Rev. Microbiol.* **2019**, *17*, 203–218.

[9] Y. Guo, G. Song, M. Sun, J. Wang, Y. Wang, *Front. Cell. Infect. Microbiol.* **2020**, 10:107.

[10] N. I. Samia, A. Robicsek, H. Heesterbeek, L. R. Peterson, *Sci Rep.* **2022**, *12*, 17007.

[11] M. Scaccaglia, M. P. Birbaumer, S. Pinelli, G. Pelosi, A. Frei, *Chem. Sci.* **2024**, *15*, 3907–3919.

[12] M. Orsi, B. S. Loh, C. Weng, W. H. Ang, A. Frei, *Angew. Chem. Int. Ed.* **2024**, *63*, e202317901.

[13] S. Fulgencio, M. Scaccaglia, A. Frei, *ChemBioChem* **2024**, *25*, e202400435.

[14] Y. C. Ong, S. Roy, P. C. Andrews, G. Gasser, *Chem. Rev.* **2019**, *119*, 730–796.

[15] T. W. Rees, P.-Yu. Ho, J. Hess, *ChemBioChem* **2023**, *24*, e202200796.

[16] F. Chen, J. Moat, D. McFeely, G. Clarkson, I. J. Hands-Portman, J. P. Furner-Pardoe, F. Harrison, C. G. Dowson, P. J. Sadler, *J. Med. Chem.* **2018**, *61*, 7330–7344.

[17] A. Marco, G. Vigueras, N. Busto, N. Cutillas, D. Bautistad, J. Ruiz, *Dalton Trans.* **2023**, *52*, 13482–13486.

[18] H.-Y. Huang, P. Wang, W. Deng, L.-X. Dou, X.-W. Liao, J.-T. Wang, X.-M. Duan, R.-J. Yu, Y.-S. Xiong, *Dalton Trans.* **2023**, *52*, 9757–9771.

[19] B. Das, P. Biswas, A. I. Mallick, P. Gupta, *Chem. Eur. J.* **2024**, *30*, e202400646.

[20] L. Jiang, Y. Ma, Y. Chen, M. Cai, Z. Wu, Y. Xiong, X. Duan, X. Liao, J. Wang, *RSC Med. Chem.* **2023**, *14*, 700–709.

[21] A. Frei, A. D. Verderosa, A. G. Elliott, J. Zuegg, M. A. T. Blaskovich, *Nat. Rev. Chem.* **2023**, *7*, 202–224.

[22] N. Jain, P. Alam, I. R. Laskar, J. Panwar, *RSC Adv.* **2015**, *5*, 61983–61988.

[23] A. Gupta, P. Prasad, S. Gupta, P. K. Sasmal, *ACS Appl. Mater. Interfaces* **2020**, *12*, 35967–35976.

[24] P.-Y. Ho, S.-Y. Lee, C. Kam, J. Zhu, G.-G. Shan, Y. Hong, W.-Y. Wong, S. Chen, *Adv. Healthcare Mater.* **2021**, *10*, 2100706.

[25] Xu, P. Deng, W. Song, M. Liu, M. Wang, Y. Yu, F. Wang, *ACS Materials Lett.* **2023**, *5*, 162–171.

[26] A. Gautam, A. Gupta, P. Prasad, P. K. Sasmal, *Dalton Trans.* **2023**, *52*, 7843–7853.

[27] A. Gupta, T. Adarsh, V. Manchanda, P. K. Sasmal, S. Gupta, *Dalton Trans.* **2023**, *52*, 1188–1192.

[28] G. Kumari, A. Gupta, R. K. Sah, A. Gautam, M. Saini, A. Gupta, A. K. Kushawaha, S. Singh, P. K. Sasmal, *Adv. Healthcare Mater.* **2023**, *12*, 2202411.

[29] M. Liu, W. Song, P. Deng, S. Nong, X. Zhang, Y. Yu, G. Li, L. Xu, *Eur. J. Med. Chem.* **2023**, *251*, 115249.

[30] Y. Zhu, C. Xu, Y. Wang, Y. Chen, X. Ding, B. Yu, *RSC Adv.* **2017**, *7*, 32632–32636.

[31] S. Gao, X. Yan, G. Xie, M. Zhu, X. Ju, P. J. Stang, Y. Tian, Z. Niu, *Proc. Natl. Acad. Sci. U. S. A.* **2019**, *116*, 23437–23443.

[32] W. H. Yu, S. C. Yiu, M. T. Lau, P. Y. Ho, P. L. Lam, C. H. Chui, W. Y. Wong, *Eur. J. Inorg. Chem.* **2023**, *26*, e202200529.

[33] M. Gao, Q. Hu, G. Feng, N. Tomczak, R. Liu, B. Xing, B. Z. Tang, B. Liu, *Adv. Healthcare Mater.* **2015**, *4*, 659–663.

[34] G. Feng, C.-J. Zhang, X. Lu, B. Liu, *ACS Omega* **2017**, *2*, 546–553.

[35] N. Busto, G. Vigueras, N. Cutillas, B. García, J. Ruiz, *Dalton Trans.* **2022**, *51*, 9653–9663.

[36] Y. Han, H.-T. Cao, H.-Z. Sun, Y. Wu, G.-G. Shan, Z.-M. Su, X.-G. Hou, Y. Liao, *J. Mater. Chem. C* **2014**, *2*, 7648–7655.

[37] C. Caporale, A. M. Ranieri, S. Paternoster, C. A. Bader, M. Falasca, S. E. Plush, D. A. Brooks, S. Stagni, M. Massi, *Inorganics* **2020**, *8*, 23.

[38] Y. Wang, Y.-T. Hu, H.-L. Zhang, Y.-Y. Chen, H.-D. Shi, J.-G. Liu, Q.-L. Zhang, *Dalton Trans.* **2023**, *52*, 8051–8057.

[39] A. Gupta, A. K. Pandey, T. Mondal, J. Bhattacharya, P. K. Sasmal, *J. Med. Chem.* **2023**, *66*, 8687–8704.

[40] C. Weng, L. Shen, J. W. Teo, Z. C. Lim, B. S. Loh, W. H. Ang, *JACS Au* **2021**, *1*, 1348–1354.

[41] X. Li, Y. Wang, M. Li, H. Wang, X. Dong, *Molecules* **2022**, *27*, 148.

[42] A. Kessler, J. Hedberg, E. Blomberg, I. Odnevall, *Nanomaterials (Basel)* **2022**, *12*, 1922.

[43] N. Singh, A. Gupta, P. Prasad, R. K. Sah, A. Singh, S. Kumar, S. Singh, S. Gupta, P. K. Sasmal, *J. Med. Chem.* **2021**, *64*, 17813–17823.

[44] A. Gupta, N. Singh, A. Gautam, N. Dhakar, S. Kumar, P. K. Sasmal, *RSC Med. Chem.* **2023**, *14*, 1088–1100.

[45] P. A. Wayne, Clinical and Laboratory Standards Institute, *Performance Standards for Antimicrobial Susceptibility Testing; Twenty-Fifth Informational Supplement*, CLSI document M100-S25,**2015**.

Manuscript received: August 24, 2024
Revised manuscript received: November 8, 2024
Accepted manuscript online: November 9, 2024
Version of record online: November 23, 2024